Engineering Geology 265 (2020) 105452

Contents lists available at ScienceDirect

Engineering Geology

journal homepage: www.elsevier.com/locate/enggeo

Modelling earthquake rupture rates in fault systems for seismic hazard assessment: The Eastern Betics Shear Zone

Octavi Gómez-Novell[a,*], Thomas Chartier[b,c], Julián García-Mayordomo[d], María Ortuño[a], Eulàlia Masana[a], Juan Miguel Insua-Arévalo[e], Oona Scotti[c]

[a] RISKNAT Group, GEOMODELS, Departament de Dinàmica de la Terra i de l'Oceà, Facultat de Ciències de la Terra, Universitat de Barcelona, 08028 Barcelona, Spain
[b] Laboratoire de Géologie, CNRS UMR8538, Ecole Normale Supérieure, PSL University, 24 rue Lhomond, 75005 Paris, France
[c] Institut de Radioprotection et de Sûreté Nucléaire, 31 avenue de la Division Leclerc, 92260 Fontenay aux Roses, France
[d] Instituto Geológico y Minero de España, 28760 Tres Cantos, Spain
[e] Departamento de Geodinámica, Estratigrafía y Paleontología, Facultad de Ciencias Geológicas, Universidad Complutense de Madrid, 28040 Madrid, Spain

ARTICLE INFO

Keywords:
Seismic hazard
Fault rupture
Annual earthquake rate
Paleoseismology
MFD
Gutenberg–Richter

ABSTRACT

Earthquake surface fault ruptures can show very complex geometries and involve different faults simultaneously. Consequently, modern fault-based probabilistic seismic hazard assessments (PSHA) need to account for such complexities in order to achieve more realistic modellings that treat fault systems as a whole and consider the occurrence of earthquake ruptures as aleatory uncertainties. We use SHERIFS, a recent approach of modelling annual rates of complex multi-fault ruptures, to obtain system-level magnitude-frequency distributions (MFDs) for the Eastern Betics Shear Zone (EBSZ, Spain) considering four fault rupture hypotheses. We then analyze the consistency of each scenario based on data from the earthquake catalogue and paleoseismic studies. The definition of the different rupture hypotheses was discussed within the frame of Fault2SHA ESC working group and critical fault input data is extracted from previous published studies. The four rupture hypotheses are defined as incremental scenarios based on fault geometry and kinematics, with lengths varying from minimal fault sections to a rupture of nearly the whole system.

The results suggest that multi-fault ruptures involving lengths up to single to several whole faults are consistent with the annual rates from both the instrumental catalogue and paleoseismic record. The method does not allow to completely discard any hypothesis, but it allows to weight the different models in a logic tree for seismic hazard assessment. The approach is revealed as a practical tool for obtaining fault-system MFDs and as a useful tool for highlighting limitations and uncertainties in geological and paleoseismic data to be assessed. This study aims to constitute a step forward in the consideration of complex multi-fault ruptures for future seismic hazard assessments in the region.

1. Introduction

Characterizing faults as seismogenic sources in probabilistic seismic hazard assessment (PSHA) is far from trivial. Field data shows that earthquake surface ruptures can be very complex, involving faults with different characteristics in a broad system (e.g., 2010 El Mayor Cucapah earthquake; Wei et al., 2011 and 2016 Kaikoura earthquake; Kearse et al., 2018). Modern fault-based PSHA models should then evolve and consider earthquakes corresponding to single-fault ruptures as well as to multi-fault ruptures that propagate through a fault system. In this sense, the occurrence of earthquake ruptures should be treated as an aleatory uncertainty linked to the randomness of the seismic process while exploring the epistemic uncertainty of which rupture is considered in each model.

Generally, seismic hazard studies have estimated earthquake parameters from instrumental or historical seismicity data, but classically, the use of fault geological data has not been widespread in source modelling (e.g. Bayrak et al., 2009), mainly due to the lack of good quality input data and efficient modelling tools. The inclusion of faults into seismic hazard calculations has been the subject of many studies as more geological results on the seismic behavior of active faults have become available. Most studies consider faults as independent sources, which accommodate the largest earthquakes from a cut-off magnitude, while the smaller ones occur in a defined buffer zone (e.g. Frankel,

* Corresponding author.
E-mail addresses: octgomez@ub.edu (O. Gómez-Novell), chartier@geologie.ens.fr (T. Chartier), julian.garcia@igme.es (J. García-Mayordomo), maria.ortuno@ub.edu (M. Ortuño), eulalia.masana@ub.edu (E. Masana), insuarev@geo.ucm.es (J.M. Insua-Arévalo), oona.scotti@irsn.fr (O. Scotti).

https://doi.org/10.1016/j.enggeo.2019.105452
Received 28 June 2019; Received in revised form 5 December 2019; Accepted 5 December 2019
Available online 09 December 2019
0013-7952/

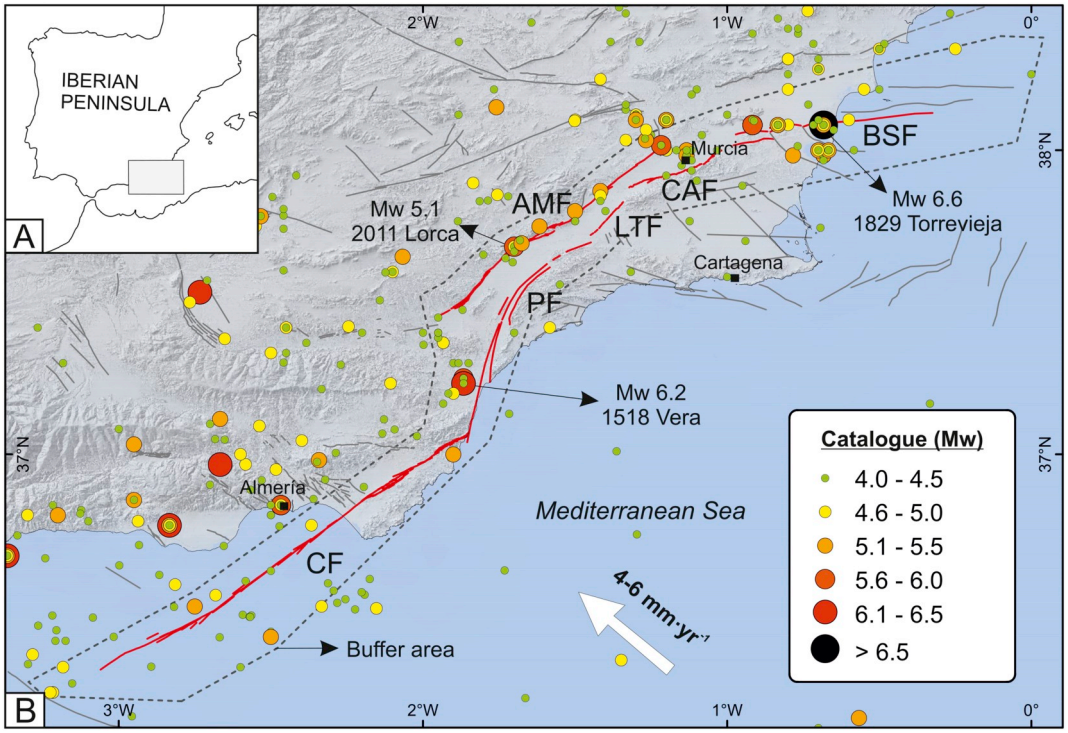

Fig. 1. A. Location of the study area within the Iberian Peninsula. B. Tectonic scheme of the Eastern Betics Shear Zone (EBSZ). Faults considered in the present study are depicted in red. CF: Carboneras fault; PF: Palomares fault; LTF: Los Tollos fault; CAF: Carrascoy fault; BSF: Bajo Segura fault; AMF: Alhama de Murcia fault. The time period covered by the earthquake catalogue extends from years 1048 to 2011 (IGN-UPM working group, 2013). The largest known historical and instrumental earthquakes within the buffer area are pointed with an arrow. (For interpretation of the references to color in this figure, the reader is referred to the web version of this article).

1995 in USA; Woessner et al., 2015 in the European SHARE project; Valentini et al., 2017 in central Italy). Geological, paleoseismological and geometrical characteristics of these faults are used to estimate the maximum magnitude (M_{max}) and the magnitude-frequency distribution (MFD) for each fault in the system, either following an exponential model (i.e., a Gutenberg–Richter distribution; Gutenberg and Richter, 1944) or a characteristic earthquake model (Wesnousky, 1986; Youngs and Coppersmith, 1985). These approaches do not contemplate the occurrence of linked fault ruptures nor the inclusion of fault complexity into the models. However, recent studies have developed system level approaches considering faults as interacting sources that can get involved in linked ruptures and taking into account fault complexities such as geometrical and slip rate variations. In addition, some of these studies consider the occurrence of multi-fault ruptures as an aleatory uncertainty linked to the randomness of the seismic process (e.g. Chartier et al., 2017, 2019; Field et al., 2014; Working Group On California Earthquake Probabilities, 2003).

The Eastern Betics Shear Zone (EBSZ; De Larouzière et al., 1988) is the longest active fault system in the Betic Cordillera (SE Spain; Fig. 1A, B) and one of the most seismically active areas in Spain (García-Mayordomo et al., 2007). From a global perspective, it is an area with low-to-moderate seismicity. However, the slip rates estimated for some faults ($> 1\ mm{\cdot}yr^{-1}$; Echeverria et al., 2015; Ferrater, 2016; Ferrater et al., 2017) underline the moderate-high seismic potential of the area and highlight the need to better constrain the probability of occurrence of potentially damaging earthquakes. The EBSZ is a complex fault-system composed by an ensemble of faults with contrasting geometries and slip rate variations (Ferrater et al., 2017).

In past PSHA studies, the EBSZ has been modelled as a source zone following the Cornell-McGuire methodology (Cornell, 1968; McGuire, 1976), delineating the territory in zones and obtaining a magnitude-frequency distribution (MFD) from the earthquake catalogue of the area (Gaspar-Escribano et al., 2008, 2015). Other studies have modelled PSHA in terms of Arias intensity (e.g. Peláez et al., 2005). Later on, it has been modelled incorporating major faults as a set of independent segments, considering either a characteristic earthquake model (e.g. Wesnousky, 1986) or an exponential MFD based on geological data (e.g. fault dimensions and slip rate; García-Mayordomo, 2005; García-Mayordomo et al., 2007). For the official seismic hazard map of Spain (IGN-UPM working group, 2013) the EBSZ was modelled as a seismogenic zone, consistently with the zoning model used in the rest of Spain, because at that time the available fault data was neither representative or complete for the whole territory (García-Mayordomo, 2015). More and higher precision paleoseismic parameters are available nowadays thanks to several paleoseismic studies conducted in the last decade (e.g. Ferrater, 2016; Insua-Arévalo et al., 2015; Martín-Banda et al., 2015; Martínez-Díaz et al., 2018). Recently, Rivas-Medina et al. (2018) proposed a hybrid approach that avoids setting an arbitrary cut-off magnitude for distributing seismic moment between faults and zones and, at the same time, ensure that this distribution of seismic potential is not double-counted. This is achieved by computing and distributing the seismic potential between faults and zones using the events contained in the completeness period of the catalogue for different magnitude ranges. However, so far no attempts have been done to address and model the occurrence of multi-fault ruptures at the EBSZ with a system-level approach, as we present.

In this work, we use the SHERIFS code (Seismic Hazard and Earthquake Rates in Fault Systems; Chartier et al., 2019) to generate synthetically derived MFDs for different fault and multi-fault rupture hypotheses or scenarios at the EBSZ and considering the occurrence of such possible ruptures in each hypothesis as an aleatory uncertainty. The aim of the study is to compare the synthetic MFDs with respect to the earthquake rates calculated using the earthquake catalogue and paleoseismic data. The fit between the modelled rates and the rates from the data can be used as criteria for weighting the different input hypotheses for PSHA. To do so, we first define and explore four fault

and multi-fault rupture hypotheses or scenarios at the EBSZ and we use geological fault data from previous published studies as inputs for the calculations, filtered after a thorough discussion (extended in the Appendix A). The identification of the epistemic uncertainties related to the definition of the input hypotheses and the discussion of the reliability of the fault data are further objectives of this paper, since these affect the results. It should be acknowledged that the input hypotheses presented here are based on expert criteria and that geological fault data are not always conclusive, hence expert decisions needed to be taken in some cases.

The approach used is an alternative to other studies that model earthquake recurrence considering fault data and its uncertainties (e.g. Wang et al., 2012). The rupture rates calculated and discussed in this study as well as the weighting of the different rupture hypotheses might be useful in future PSHA studies. Also, they might be used for choosing specific earthquake scenarios for neodeterministic seismic hazard calculations (NDSHA) (e.g. Magrin et al., 2017; Rastgoo et al., 2018).

2. Geological and seismological setting

The EBSZ is a 400 km long active fault system located in SE Iberia dominated by SW-NE left-lateral strike slip faults, some of which are oblique reverse faults. From SW to NE the main faults in the area are named as (Fig. 1B): Carboneras fault (CF), Palomares fault (PF), Alhama de Murcia fault (AMF), Los Tollos fault (LTF), Carrascoy fault (CAF) and Bajo Segura fault (BSF) (Alfaro et al., 2012a; Bousquet, 1979; De Larouzière et al., 1988; Insua-Arévalo et al., 2015; Martínez-Díaz et al., 2012a; Masana et al., 2004; Silva et al., 1993; among others). These faults accommodate a large portion of the shortening resulting from the convergence of the African and Nubian plates in Iberia since late Neogene (Bousquet, 1979; Martínez-Díaz, 1998; Masana et al., 2004), estimated in 4–6 mm·yr^{-1} following a N150° horizontal shortening direction (Argus et al., 2011; Demets et al., 2010).

Several studies at the EBSZ (e.g. Ferrater, 2016; Insua-Arévalo et al., 2015; Martín-Banda et al., 2015; Martínez-Díaz et al., 2003, 2018; Masana et al., 2004, 2018; Moreno, 2011; Ortuño et al., 2012) have evidenced the occurrence of recurrent morphogenetic earthquakes. Recent studies have also proposed considerably high slip rate values for some of these faults: 1.0 ± 0.2 mm·yr^{-1} (paleoseismological 3D trenching) and 1.6–1.7 mm·yr^{-1} (geomorphological analysis) for AMF (e.g. Ferrater, 2016; Ferrater et al., 2017, respectively). Remarkably, for some faults such as the northeastern section of AMF (AMF-4; Table 1), slip rate values are subject to large uncertainties, since they are estimated from long term uplifts (Herrero-Barbero, 2016).

The EBSZ is one of the most seismically active areas of Spain and it has produced some of its largest historical events (e.g. 1829 Torrevieja earthquake; Fig. 1B) with important damage effects (e.g. Delgado et al., 2011). In addition, recent earthquakes such as the M_w 5.1 ± 0.1 2011 Lorca earthquake (IGN-UPM working group, 2013) also caused great damage and related slope effects (Alfaro et al., 2012b). Most of the earthquakes in the EBSZ occur at depths < 20 km (Martínez-Díaz, 1998) and some historical events are thought to be caused by its main faults (e.g. BSF for the 1829 Torrevieja event; Alfaro et al., 2012a or AMF for the 1674 Lorca event; Martínez-Díaz et al., 2018). Even though there are not known descriptions of surface ruptures during the historical period, paleoseismic studies have demonstrated the occurrence of at least one historical surface rupturing earthquake along the EBSZ (i.e. 1674 Lorca event; Martínez-Díaz et al., 2018).

3. Datasets and methodology

To accomplish our main objectives, we set up possible multi-fault rupture scenarios in the study area and selected the slip rate data on faults from published studies following a critical revision in specific cases (see Appendix A). Then we used the SHERIFS code to model MFDs at the whole EBSZ fault system scale and analyzed the consistency of the models with data from the catalogue and paleoseismic studies.

3.1. Definition of fault rupture hypotheses

We defined four possible fault and multi-fault rupture scenarios for the EBSZ system as sets of incremental fault rupture lengths starting from minimal fault sections, which correspond to the segmentation proposed for each fault in the literature (Fig. 2A). These scenarios represent plausible rupture possibilities according to our criteria and the available data, but other could be tested.

The different hypotheses are explorative and the length of ruptures in the different scenarios was defined by imposing selected fault characteristics as barriers for rupture propagation. In our case, only geometry (mainly sense of dip) and kinematic changes between major faults or groups of faults were used as criteria to explore multi-fault rupture propagation in the different hypotheses (see more details on the specific criteria used in Section 3.1.1). In the case of AMF though, it was considered that the fault cannot rupture with any fault of the system in any hypothesis, since it dips towards the NE (Martínez-Díaz et al., 2012b) and this makes incompatible its linked rupture with the rest of faults of the system. Other fault parameters frequently used as barriers for fault rupture propagation (e.g. Boncio et al., 2004; Field et al., 2014; Wesnousky, 2008) were not contemplated in this study as we explain below.

Changes in strike and distance between faults (gaps, stepovers) were not considered as a limiting factor for rupture propagation, since they are not significant enough, considering the criteria applied in California (UCERF-3; Field et al., 2014). Neither slip rate variations along strike were used as barriers, even if these are important. This is consistent with observations on earthquakes such as the 2016 M_w 7.8 Kaikoura earthquake where > 20 faults ruptured together, some of them with extremely different slip rates (e.g. 1–2 mm·yr^{-1} for the Papatea fault and 24 ± 12 mm·yr^{-1} for the Kekerengu fault; Langridge et al., 2018 and Little et al., 2018, respectively).

Finally, the aspect ratios between fault length and width were not taken as a limiting factor for the occurrence of long fault ruptures in our models, since there is not a clear threshold for these parameters in large or extreme events, especially for strike-slip regimes. For instance, the 1906 M_w 7.9 San Francisco earthquake or the 1958 M_w 7.77 Alaska earthquake implied rupture lengths of 470 km and 260 km, respectively (Schwartz, 2018) with seismogenic widths of 12 km (Wells and Coppersmith, 1994) comparable to the EBSZ (Table 1). Also, it can be observed from the regressions in Leonard (2010) that, in strike-slip faults, for rupture lengths > 50 km the width becomes constant at a mean of 17 km, but the dataset shows large dispersion in this range and a significant amount of large ruptures (> 100 km long) are found in widths similar to the EBSZ.

3.1.1. Fault rupture hypotheses

For the modelling we only considered the main active major faults of the area (Fig. 1B), although other minor faults are known and have been studied to different degrees (e.g. faults identified by Pedrera et al., 2012).

The major faults considered are divided in shorter sections based on their geometry, geomorphic expression and seismicity in the literature, as well as on their kinematics and activity evidence. Offshore segmentation of CF was adopted from Moreno (2011), while onshore was based on García-Mayordomo (2005), same as for PF. Segmentation of CAF was adopted from Martín-Banda et al. (2015), BSF from Alfaro et al. (2012a) and AMF from Martínez-Díaz et al. (2012b).

The segmentation for each of these faults was applied to define the minimal sections (hypothesis 1) that in the subsequent hypotheses are linked to generate larger ruptures; 'multi-fault ruptures' henceforth. The fault system geometry considered is shown in Fig. 2A. Mainly for AMF-1, AMF-2, CF and PF we simplified fault sections with several parallel traces or splays to a single trace representative of the overall

Table 1
Faults data used for the MFD calculation with the SHERIFS code.

Geological fault parameters used for the modelisation										
Fault name	Fault section ID	Dip (°)	Main kinematics	Seismogenic depth (km)		Fault length (km)	Net slip rate (mm·yr^{-1})			Type of information used to infer slip rate (references) and time frame covered
				Upper	Lower		Min.	Mean	Max.	
Carboneras fault (CF)	CF-1	90	Strike-slip	0	11.0	39.1	1.1	1.2	1.3	Displaced onshore fluvial/submarine channels, trench offsets in fluvial channels and GPS data (Echeverria et al., 2015; Moreno, 2011); since Pliocene - Holocene.
	CF-2	90	Strike-slip	0	11.0	59.6	1.1	1.2	1.3	
	CF-3	90	Strike-slip	0	11.0	39.5	1.1	1.2	1.3	
Palomares fault (PF)	PF-1	90	Strike-slip	0	8.0	41.1	0.01	0.04	0.08	Tectonic uplift of terraces and alluvial fans (García-Mayordomo, 2005 and references); since lower-middle Pleistocene.
	PF-2	90	Strike-slip	0	8.0	18.5	0.01	0.04	0.08	
	PF-3	90	Strike-slip	0	8.0	21.1	0.04	0.1	0.16	Analogy with LTF and PF-2 (expert opinion; see Appendix A).
Los Tollos fault (LTF)	LTF	85	Strike-slip	0	8.0	16.0	0.06	0.16	0.25	Recurrence intervals in paleoseismological trenches (Insua-Arévalo et al., 2015); since 12 kyr.
Carrascoy fault (CAF)	CAF-1	70	Reverse	0	12.0	18.2	0.29	0.37	0.45	Restoration of deformed units, consistent with offsets in trenches (Martín-Banda et al., 2015); since 209.1 kyr.
	CAF-2	85	Strike-slip	0	12.0	13.1	0.48	0.53	0.58	Tectonic uplift of sedimentary units (based on unpublished research; see Appendix A); since 160 kyr.
Bajo Segura fault (BSF)	BSF-1	60	Reverse	1.0	12.0	11.6	0.25	0.33	0.41	Tectonic uplift of continental units (Alfaro et al., 2012a); since 2–3 kyr.
	BSF-2	60	Reverse	1.0	12.0	9.2	0.25	0.33	0.41	
	BSF-3	60	Reverse	1.0	12.0	7.7	0.12	0.2	0.3	
	BSF-4	60	Reverse	1.0	12.0	29.3	0.12	0.2	0.3	Assigned by analogy to BSF-3 section (expert opinion; see Appendix A). Consistent with new GPS results (Borque et al., 2019).
Alhama de Murcia fault (AMF)	AMF-1	70	Strike-slip	0	12.0	34.1	1.6	1.65	1.7	Displaced fluvial channels (Ferrater, 2016; Ferrater et al., 2017); since 200 kyr for AMF-1, 30 kyr for AMF-2.
	AMF-2	70	Strike-slip	0	12.0	19.7	0.8	1.0	1.2	
	AMF-3	70	Strike-slip	0	12.0	11.3	0.01	0.07	0.1	Based on expert opinion from the QAFI database (see Appendix A).
	AMF-4	45	Strike-slip	0	12.0	23.9	0.07	0.2	0.37	Tectonic uplift of sedimementary units (Herrero-Barbero, 2016); since late Miocene-Pliocene.

Slip rate data was extracted from the main studies on the faults. The type of information from where slip rates have been inferred in their respective references are indicated, although more details are explained in the Appendix A of this paper. Fault sections ID are mapped in Fig. 2A.

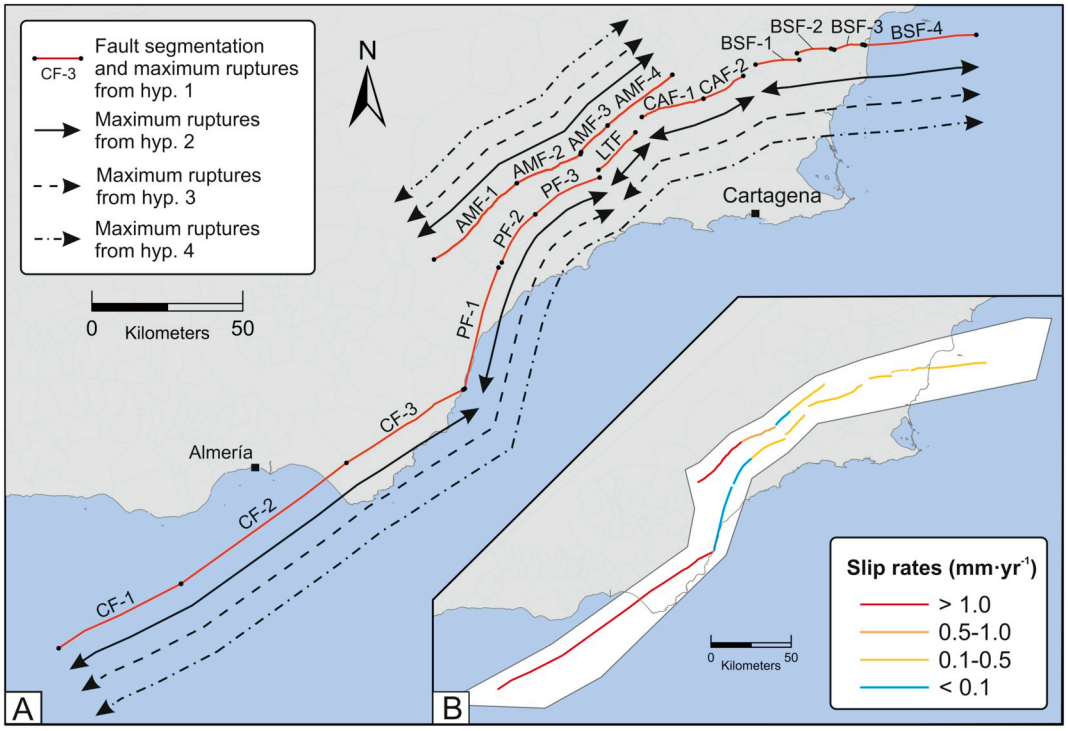

Fig. 2. A. Simplified fault traces of the main active faults in the EBSZ used in this study (extracted from the Quaternary Active Faults Database of Iberia; IGME, 2015a) and sections defined for each one of the major faults. Each fault section is codified with an ID corresponding to the abbreviation of the fault and the number of the section (see Table 1 for the assignation of the section ID to major faults). The extension of the maximum fault ruptures allowed in each rupture hypothesis is shown. B. Slip rate ranges of the EBSZ faults depicted following a colored scale. The buffer area considered is indicated. (For interpretation of the references to color in this figure, the reader is referred to the web version of this article).

geometry (Fig. 1B). This was done because fault branches likely link at depth, as suggested by Martínez-Díaz et al. (2012b) for AMF or Moreno (2011) for CF, and fault parameters of the simplified fault traces result from the merging of the individual fault branches; slip rates of CF, AMF-1 or PF are inferred from geomorphological estimations accounting for all branches. Moreover, in CF they are consistent with geodetic data (Table 1 and Appendix A).

The main difference between the hypotheses considered is the length of the maximum fault ruptures allowed. One hypothesis considers only single-section fault ruptures and the other three allow multi-fault ruptures at different extents (Fig. 2A):

Hypothesis 1 (hyp. 1). The length of the segments in the segmentation from the literature (Table 1) set the maximum length of ruptures (Fig. 2A) and multi-fault ruptures with the neighboring sections are not allowed. This follows the classical segmentation model in which is considered that earthquakes are usually confined within specific segments of a certain fault (Schwartz and Coppersmith, 1984).

Hypothesis 2 (hyp. 2). The maximum length of ruptures allowed in this hypothesis is that of complete major faults. Neighboring fault sections can rupture together within a same fault, but complex ruptures between different major faults are not envisaged. For example, the whole CF can rupture at a time, but it cannot rupture with its adjacent section of PF (Fig. 2A). In this case we assumed that geometry and kinematic characteristics that lead to define the limits between major faults in the literature act as barriers for fault rupture propagation.

Hypothesis 3 (hyp. 3). This hypothesis allows linked ruptures between selected major faults with similar geometries and kinematics, while these are excluded between faults with less similarities on these parameters. This leads to the definition of three sub-systems, within which multi-fault ruptures are allowed, but not between them (Fig. 2A). We propose a CF-PF sub-system, a LTF-CAF-BSF sub-system and an AMF sub-system. The first one is characterized by vertical dipping left-lateral strike-slip faults (Table 1). The second one is formed by predominantly high angle S-SE dipping faults with mainly reverse components (CAF and BSF). LTF, although being classified as mainly strike-slip, it has been considered within this sub-system because it limits the southern part of the mountain range uplifted by CAF suggesting its relationship with this fault. In addition, ongoing research in the area identified fault branches related to LTF with strong reverse components. The third sub-system is formed by AMF, a strike slip NW dipping fault.

Hypothesis 4 (hyp. 4). No restrictions are made in this hypothesis from CF to BSF (Fig. 2A). We considered that given a particular event, a rupture could propagate across both systems. On the other hand and as for hyp. 3, AMF is considered apart due to its contrastingly opposite sense of dip compared to the rest of the faults.

3.2. Geological fault parameters as inputs for the calculations

A current challenge in the EBSZ is the difficulty to have a complete and reliable dataset of fault geological parameters for all its major faults, such as slip rates and rates of large earthquakes. Most paleoseismological studies have typically focused on specific branches of major faults while some of the faults remain poorly studied to date. This causes heterogeneity on how the knowledge on faults is distributed. Accordingly, constraining the geological parameters for some of the faults considered is a difficult task and, for our modelling purposes, it required taking a number of assumptions and extrapolating data among different fault sections (see Appendix A).

For this reason, we emphasized the revision of the slip rates on the EBSZ faults after discussion in the frame of the Fault2SHA-Betics working group at the Eastern Betics (García-Mayordomo et al., 2018), focusing on the less studied structures.

3.2.1. Slip rates

The slip rates and uncertainties of the faults were directly obtained from published geological and paleoseismological studies, although the methods to infer them vary between studies (Table 1 and Appendix A). Slip rate data are inferred mainly from the displacement of geological markers, but for different time periods depending on the fault. CF has additional slip rates coming from geodetic measures consistent with geological estimations (Table 1).

Geological slip rates on faults have been assumed to be seismic slip rates in this study. We are aware that part of the slip rates considered may result partially from aseismic slip and it is one of the uncertainties. However, we do not think that the contribution of the aseismic slip in the EBSZ faults is that relevant because: i) Creeping is usually associated with high levels of microseismicity (Malservisi et al., 2005; Scholz, 1990), which are not found at the EBSZ. ii) Creep tends to be highly localized at the surface and creeping faults tend to lack large brittle-deformation structures and lack deposits resulting from coseismic movements (colluvial wedges, etc.) (McCalpin, 1996). Contrarily, the EBSZ faults show many evidences of brittle deformation that splay upwards to the free surface, indicating rapid deformation (e.g. as seen in trenches by Ferrater, 2016; Martín-Banda et al., 2015; Martínez-Díaz et al., 2018). iii) There is no evidence of historical offsets, even small, in anthropic structures (walls, roads, etc.) that may be hundreds of years old and cross the traces of the faster faults (i.e. AMF, CF). They should be displaced if creep was dominant or even half of the total slip rate.

Stich et al. (2007) suggest that only ~24% of the total slip rate in the Betic-Alboran-Rif area is explained by the instrumental catalogue seismicity over a 21 year period, and that the remaining 76% might be generated in either aseismic processes or be accumulating as elastic deformation, but there is no way to distinguish among these two processes. We think that an important part of that 76% might be released as large seismic events, considering that the EBSZ is a low-strain region and that the last large events are previous to the 20th century (e.g. 1829 Torrevieja and 1674 Lorca earthquakes). Paleoseismic results in the area evidence that faults have much larger recurrence intervals than the time window of the seismic catalogue.

As it can be seen in Fig. 2B and Table 1, slip rate values are remarkably different from one source to another. The faults that have higher slip rate values are those that have been object of most paleoseismological, geomorphological and geodetic studies during the last decades (i.e. AMF-1 and 2, CF) and thus have better constrained geological parameters with lower uncertainty intervals. Conversely, faults that have been object of very few or no paleoseismological and geodetic studies have systematically lower estimated slip rate values. This has to do with the fact that their slip rates are mainly based on the long-term uplift of mountain fronts and sedimentary units (i.e. PF-1 and 2, BSF-1 to 3, CAF-2, AMF-4). As a result, the net slip rate is inferred from the vertical slip rate (Table 1), which carries large uncertainties. The time frame of this data is much longer than for the other faults and the kinematics of some sections are not clear.

Due to lack of data, for the cases of PF-3, CAF-2, BSF-4 and AMF-3, slip rate values were established following a number of geological expert criteria explained in the Appendix A. The details and the type of geological information used by each study to infer the slip rate of each individual fault are also explained there.

3.2.2. Paleorates

Annual rates of large earthquakes or paleoearthquakes (paleorates) were inferred from minimum and maximum recurrence intervals published in the available paleoseismic literature from trench data. Mean values have been calculated for each different recurrence distribution (Table 2). The methods used to infer such paleorates in each published study are indicated in Table 2 and detailed in the Appendix A. These data are considered when comparing the SHERIFS models with the geological information in the discussions.

For all cases, the magnitude of the paleorates for all faults was assumed to be a minimum of M_w 6.25 ± 0.25. This threshold was selected because statistically, earthquakes of $M_w < 6.0$ are <50% likely to rupture the surface (Biasi and Weldon, 2006) and hence to be recorded as fault ruptures in the paleoseismic record. Data by Bonilla (1982), McCalpin (1996) or the Unified Database of Surface Ruptures (SURE; Baize et al., 2019) support this selection. Additionally, very shallow earthquakes at the EBSZ such as the M_w 5.1 ± 0.1 2011 Lorca earthquake (IGN-UPM working group, 2013) have not ruptured the surface, and events identified in trenches, despite the uncertainties of these estimations, infer slips per event consistent with $M_w > 6.0$ (e.g. Ferrater, 2016; Moreno, 2011).

3.2.3. Other parameters

Geological parameters of the faults such as dip, kinematics, fault traces, length and seismogenic depth were extracted from the Quaternary Active Faults of Iberia database (QAFI) (García-Mayordomo et al., 2012, 2017; IGME, 2015a), which compiles the data on the literature from each fault. Exceptionally, for PF we used the kinematics proposed by Roquero et al. (2019), since it is more recent (Table 1). However, García-Mayordomo (2005), as compiled in the QAFI database, considers PF as a dip slip fault and the net slip rate estimations are inferred from this consideration. Hence, it is important to recognize that the net slip rate for this fault is a minimum and it is subject to large uncertainty as it strongly depends on its kinematics, which are still not clear. Although these discrepancies, our modelling does not rely on the kinematics of the fault since the scaling law used is valid for all types (see Section 3.3.1).

3.3. SHERIFS method

The flexibility of the SHERIFS methodology makes it well suited for regions where seismic and geodetic data are insufficient to characterize the activity of faults and hence geological data is the prime source of information on fault characteristics, long-term behavior and seismic potential, as it is the case of the EBSZ.

SHERIFS treats the slip rate of each individual fault of the system as a budget, which is consumed by the iterative steps of the method and converted into rates of earthquakes assuming a given shape of a target MFD set at the fault system level. Iteratively, SHERIFS picks a magnitude according to the target MFD and picks a rupture whose size corresponds to this magnitude. An increment of the slip-rate budget of the faults involved in this rupture is converted into earthquake rate. The iterative process goes on until the slip-rate budget of limiting faults is exhausted. See Chartier et al. (2019) for details on SHERIFS iterative process and how the target MFD is set.

In some cases, in order to fit the target MFD, not all the slip rate can be converted into seismic moment rate and the remaining slip rate budget (called Non-Main-Shock slip or NMS) can be considered as either post-seismic re-adjustments or creep, or a modelling error. This NMS has important implications in the models; a high NMS proportion is likely a suggesting a modelling error due to an incompatibility between data, target MFD and rupture hypotheses. For example, the slip-rate value of some fault cannot be converted into seismicity rates with a given set of rupture hypotheses while respecting the target MFD shape. However, a NMS value different than zero is not necessarily a modelling incompatibility and can reflect the possibility for some faults to spend a non-negligible amount of their slip-rate as non-seismic processes such a post-seismic creep.

The required geological inputs of the SHERIFS method are: i) a 3D geometry of the fault system, ii) a list of potential fault sources (i.e. individual fault sections) and iii) the slip rate range of each individual fault. Additionally, the calculation process requires to set up iv) a specified target shape for the MFD of the fault system (e.g. the b value of a Gutenberg–Richter), v) a scaling relationship to estimate the magnitude of ruptures, vi) the minimum magnitude of earthquakes

Table 2
Recurrence intervals extracted from the paleoseismological studies and cummulative annual rates of paleoearthquakes ($M_w \geq 6.25 \pm 0.25$) inferred from these studies.

Paleoearthquake rate estimations							
Studies	Recurence interval (kyr)		Cummulative paleoearthquake rate (eq/yr)			Fault section ID	Type of information used to infer recurrence
	Min.	Max.	Min.	Mean	Max.		
Ferrater (2016)	2.0	5.3	1.89E-04	3.44E-04	5.00E-04	AMF-2	Age constraints of paleoevents in trenches.
Insua-Arévalo et al. (2015)	2.2	6.86	1.46E-04	2.44E-04	4.55E-04	LTF	
Martín-Banda et al. (2015)	2.6	4.0	2.50E-04	3.08E-04	3.85E-04	CAF-1	
Moreno (2011)	1.15	13.8	7.25E-05	1.96E-04	8.70E-04	CF-3	
Ortuño et al. (2012)	15.0	29.0	3.45E-05	4.71E-05	6.67E-05	AMF-1	
Martínez-Díaz et al. (2018)	0.34	3.12	3.21E-04	7.97E-04	2.96E-03	AMF-1	Maximum magnitude model

The types of information used for the calculation of the recurrence values in each study are indicated (see the Appendix A for details) as well as the fault sections where these studies developed; see Fig. 4 for map location. Values are rounded to two decimal digits.

produced by the faults that would be of interest for the seismic hazard assessment and vii) different hypotheses/scenarios of fault and multi-fault ruptures.

The method allows to explore the epistemic uncertainties of the parameters involved in the calculations (e.g., fault slip rate, maximum magnitude of rupture, b-value of the MFD target shape, etc.) by sampling them randomly in order to produce n (n = 20 in our study) models of annual earthquake rates for each multi-fault rupture hypothesis considered.

Finally, each modelled MFD of each rupture hypothesis is compared to the seismicity rates from the regional catalogue and the paleorates deduced from paleoseismological studies (Figs. 3 and 4). Furthermore, based on the outcome of this check, SHERIFS allows to incorporate a weight to each resulting model; we suggest weighting the four multi-fault rupture scenarios in order to consider their epistemic uncertainty in a logic tree for future PSHA calculations.

3.3.1. Model parameters

Wells and Coppersmith (1994) for rupture area and 'all type of kinematics' was used to calculate the M_{max}. A shear modulus of 30 GPa was assumed representative for the calculation of seismic moment in the area. For the computation of each MFD, twenty random samples of

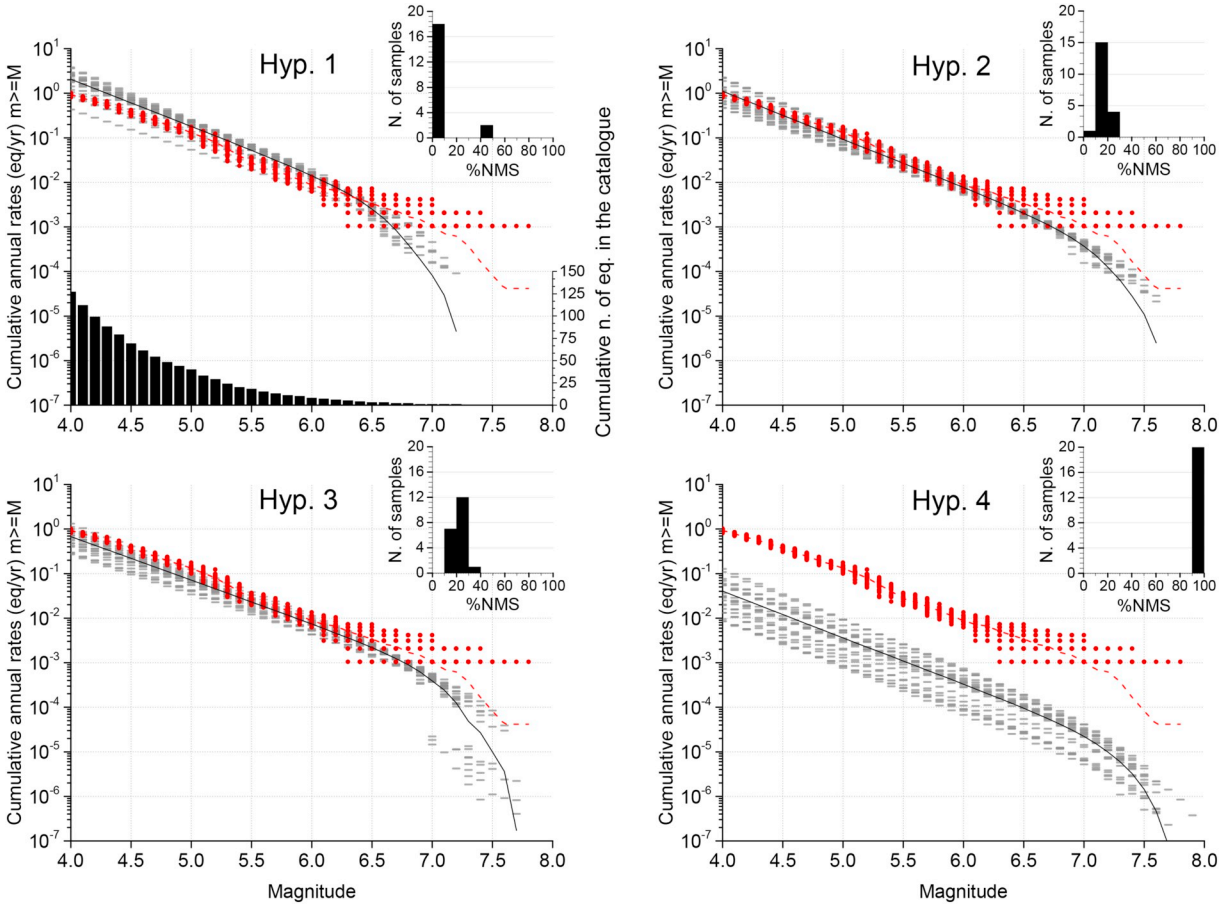

Fig. 3. Comparison between the GR curves modelled with SHERIFS for each hypothesis (grey) and the earthquake rates from the catalogue (red point cloud). Mean GR curve modelled: solid black line; samples modelled: short grey lines; mean GR curve of the catalogue: red dashed line. The bottom of the hyp. 1 graph shows the cumulative number of earthquakes of the catalogue per magnitude used to draw its MFD. Non-Main-Shock slip (NMS) histograms of the resulting models are indicated. (For interpretation of the references to color in this figure, the reader is referred to the web version of this article).

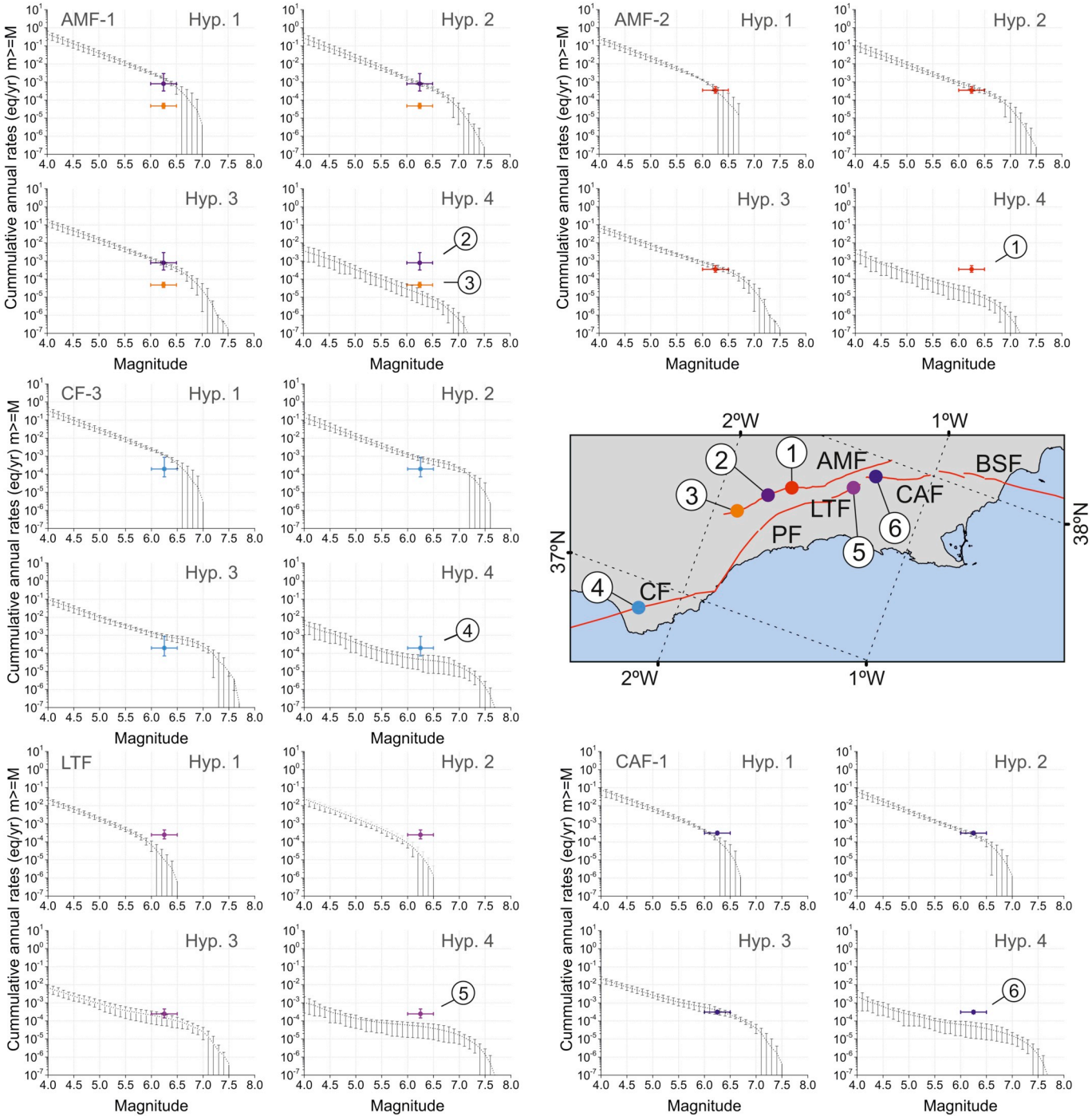

Fig. 4. Annual rates of paleoearthquakes with their uncertainty ranges inferred from paleoseismological studies. These are plotted together with the modelled GR curves of their respective fault sections (participation rates) and for each rupture hypothesis. A fault map with the location of the paleoseismic studies (colored points and their respective numbers) in each fault section is included. 1: Ferrater (2016); 2: Martínez-Díaz et al. (2018); 3: Ortuño et al. (2012); 4: Moreno (2011); 5: Insua-Arévalo et al. (2015); 6: Martín-Banda et al. (2015). Paleoearthquake rate values are available in Table 2. (For interpretation of the references to color in this figure, the reader is referred to the web version of this article).

the slip rate on faults, the b-value and M_{max} were explored. Minimum magnitude (M_{min}) was set at M_w 4.0, since below that magnitude earthquakes are not likely to be damaging and therefore not of interest for a hazard model. We assume all the seismicity over M_w 4.0 within the buffer area defined in Fig. 1B to be related to the studied fault system, because it is a narrow area (~30 km wide; Fig. 1B) constrained to the surface projection of the major faults of the EBSZ. In this sense, Stich et al. (2010) obtain moment tensors calculated on the Betic-Alboran shear zone for the 2005–2008 period (all $M_w < 5.0$ at the EBSZ) that are compatible with the main kinematics of the EBSZ major faults. Out of this period, other $M_w < 5.0$ earthquakes show compatible moment tensors and are also related to these faults, as highlighted by Martínez-Díaz et al. (2012b) for AMF (e.g. 1977 M_w 4.2, 2000 M_w 3.7, 2000 M_w 3.8 and 2011 M_w 4.8 Lorca earthquakes). Despite this, we are aware of the possible limitations of assuming all seismicity happening on the known faults, because earthquakes, especially lower magnitudes, may occur out of their extent (Fig. 1B). However, it is important to consider that a big part of the catalogue for $M_w \geq 4.0$ at the EBSZ is pre-

Table 3
Completeness years of the earthquake catalogue in SE Spain (IGN-UPM working group, 2013).

Earthquake catalogue	
Magnitude range	Year of completeness
3.0–3.4	1978
3.5–3.9	1975
4.0–4.4	1908
4.5–4.9	1883
5.0–5.4	1800
5.5–5.9	1520
≥ 6.0	1048

instrumental and historical, which implies that the location of epicenters is subject to significant uncertainty.

The earthquake catalogue used to check the synthetic MFDs is the one used in the frame of the update of the Spanish national seismic hazard map (see details in IGN-UPM working group, 2013), but without de-clustering and clearing of foreshocks and aftershocks. Moment rate budgets used in SHERIFS are based on geological slip rates, which in fact, integrate the main shocks as well as foreshocks, aftershocks, clusters aseismic slip, etc. The resulting catalogue includes 2839 earthquakes of $M_w \geq 4.0$ from year 1048 CE to June 2011. In the EBSZ, the maximum magnitude (M_{max}) corresponds to the M_w 6.6 ± 0.2 1829 Torrevieja earthquake, however, larger earthquakes could have happened given the large uncertainties in magnitude estimation of some historical earthquakes. For example, the 1518 Vera earthquake has an estimated magnitude of M_w 6.2 ± 0.8, meaning that the event could have reached magnitudes up to M_w 7.0 with a 34.1% of probability. The completeness years of the catalogue are shown in Table 3.

In order to better compare the MFDs of each scenario, only catalogue earthquakes occurring within the seismogenic crust of the EBSZ were considered, which is assumed to have thicknesses ranging from 8 to 12 km depending on the area (García-Mayordomo, 2005; Table 1). This tried to ensure that earthquakes located in this depth range were more likely produced by the faults in our study and not by deeper unidentified sources.

The buffer area used to extract the seismicity (Fig. 1B) was originally defined as an area source for the calculation of the Spanish seismic hazard map and was delineated based on the surface projection of the faults (IGME, 2015b; IGN-UPM working group, 2013). We considered an MFD target shape that follows a Gutenberg–Richter distribution (GR; Gutenberg and Richter, 1944) with a b-value in the range of 0.8–1.2, whose central value is coincident with the b-value of 1.03 assigned to the EBSZ (IGME, 2015b; IGN-UPM working group, 2013). This wide b-value range was explored in order to prevent the resulting MFDs of our hypotheses from being limited or biased by such value or imposed shape of the MFD.

See the datasets available on the Mendeley Data of this paper (Gómez-Novell et al., 2019) for more details on the SHERIFS parameters and models performed in this study, the raw inputs and output files of the calculations, including the fault parameters and the seismic catalogue used.

4. Results

4.1. Modelled earthquake rates from SHERIFS

The modelling with SHERIFS provided four MFDs for each rupture hypothesis set which refer to the whole EBSZ system (Fig. 3). Each of the four obtained GR MFDs is composed by a set of twenty samples per 0.1 magnitude increment, which form twenty different MFDs. These twenty distributions that result from the random sampling process of the input data (slip rate, M_{max} and b-value) compose the overall curve of each hypothesis.

As Fig. 3 illustrates, the hypotheses that consider larger multi-fault rupture scenarios show larger M_{max}. Annual rate values are similar for hyp. 1 to 3 in the range of M_w 4.0–6.5, while hyp. 4 shows much lower values for the whole log-linear distribution.

4.1.1. Performance of SHERIFS models

We analyze the performance of the different hypotheses in terms of the % of Non-Main-Shock slip (NMS). Its relation to the seismic moment rate describes the performance of the hypotheses in SHERIFS. From hyp. 1 to 3, >70% of the slip rate is converted into seismic moment rate, and thus only 30% of the slip is assumed as NMS for most of the samples on the slip rate and M_{max} (Fig. 3). On the other hand, in hyp. 4, only 10% of the slip rate (i.e. 90% of NMS) is converted into seismic moment rate and hence it does not perform as well as the other hypotheses.

We explain the %NMS in our models as a consequence of the configuration of ruptures of each hypothesis in relation to the slip rate variations between fault sections. This configuration affects how the slip rate budget is consumed in the different iterations of the modelling.

The fact that large multi-fault ruptures involve slower sources, causes their slip rate budget to be rapidly exhausted in the highest magnitude ruptures, since they are the ones that consume most seismic moment rate. When this happens, the target MFD of the system is set and the rest of the calculation follows this imposed shape. In the case of the EBSZ, the rates of very large ruptures (i.e. hyp. 4) are significantly low because they are limited by slow moving faults (e.g. PF, LTF, CAF, BSF; Fig. 2B, Table 1). When the target is set in the high magnitudes, the rates of the whole distribution are therefore lowered. Consequently, for such large rupture scenarios the system has a lot of remaining slip rate budget not converted into seismic moment (i.e. NMS). This NMS is hosted by the faster faults, which are the ones whose budget is not exhausted. Such effect also evidences the fact that the poor knowledge on the slip rate for some of the faults, i.e. the ones with lower slip rates, especially PF (Table 1), limits the way the models consume their budget and the resulting MFDs. Thus, it is critical to constrain them in future paleoseismic studies.

Because NMS cannot be directly interpreted as a nature-related effect, but as an artefact of the model linked to the rupture hypotheses, MFD target and input data set, we use it to evaluate the adequacy of our hypotheses. In the line of Chartier et al. (2019), we have set a threshold of 30% NMS for the overall system as an indicator of models that are not sufficiently satisfactory. This value is in agreement with studies that estimate that post-seismic moment release reaches at most 30% of the total moment released in seismic events. The normal faulting M_w 5.9 1999 Athens earthquake, for instance, was interpreted to have released aseismically 30% of the total moment (Baumont et al., 2004). The strike-slip faulting M_w 5.6 1979 Homestead and the M_w 7.5 1992 Landers earthquakes in California showed estimated post-seismic releases of about 10–15% (Shen et al., 1994; Stein and Lisowski, 1983, respectively).

Hypotheses 1–3 have 80–90 to 100% of their samples below 30% of NMS (Fig. 3), hence it could be interpreted as part of the slip rate that is not consumed seismically. Conversely, the high %NMS of hypothesis 4 suggests that the fault rupture configuration is not adequate given the methodology and fault input data and hence, a modelling error is detected. This is also evidenced by the high dispersion of the log-linear GR curve of this model compared to the others.

4.2. Comparison with the earthquake catalogue and paleoseismic data

4.2.1. Seismicity rates from the earthquake catalogue

We visually analyzed the fit between the SHERIFS MFDs and the annual seismicity rates obtained from the regional earthquake catalogue (IGN-UPM working group, 2013). Note that the GR curve from the catalogue covers a dispersed range of annual rates due to the

exploration of the code within the magnitude uncertainty of the events in the catalogue (Fig. 3). The dispersion is higher for the high magnitudes ($M_w \geq 6.0$) due to the large uncertainties related to the magnitude estimation of large historical events at the EBSZ.

The MFD from hyp. 2 shows the better fit with the seismicity rates especially for M_w 4.0–6.0 (Fig. 3). MFDs from hyp. 1 and 3 show similar good agreements with the catalogue as well, but their fit is poorer; hyp. 1 slightly overestimates the catalogue, while hyp. 3 underestimates it. The curve from hyp. 4, on the other hand, shows a strong disagreement with the seismic catalogue, where the rates modelled highly underestimate the seismicity rates (Fig. 3).

4.2.2. Paleorates

Annual earthquake rates from paleoseismological research at the EBSZ (see Table 2) were compared with the modelled curves for the $M_w \geq 6.0$ range. (Fig. 4). The paleorates from each paleoseismological study (Table 2) are plotted together with the participation rates of each corresponding fault section for each rupture hypothesis (Fig. 4). These GR curves show the participation rates resulting from considering all the ruptures hosted in each fault section per rupture scenario.

As it is observed from the plotted figures (Fig. 4), hyp. 4 does not match the paleorates estimated from the studies at the EBSZ. Hyp. 2 and 3, on the other hand, predict better the inferred paleorates for most of the faults considering their uncertainties. In most cases, the differences between these two hypotheses are barely noticeable, as it is the case of the paleorates of CF, AMF-2 and CAF-1, but for LTF hyp. 3 has the better fit (Fig. 4), since both hyp. 1 and 2 assume the same rupture model for this fault (Fig. 2A). The participation rates from hyp. 1 show, in some sites, good results with the paleorates, especially in AMF-2, but not superior than hyp. 2 and 3. Note also that the paleorates of AMF-1 by Ortuño et al. (2012) do not fit the modelled rates, as we discuss in Section 5.1.2.

5. Discussion

5.1. Analysis of the modelling results with the datasets

5.1.1. Seismicity rates from the catalogue

The better fits of the seismic catalogue with hyp. 2 especially, but also hyp. 1 and 3 (Fig. 3) do not allow determining if these hypotheses describe the manner in which the EBSZ system works. They only show that, given the methodology used, the input data and the rupture hypotheses explored, the models are more consistent with the low-moderate magnitude seismicity of the EBSZ than others. Hence, no hypothesis should be ruled out, especially considering the epistemic uncertainties linked to some slip rate estimations. However, the consistency of these models can be used to guide their weight in a logic tree for PSHA.

Overestimation of the seismicity rates by hyp. 1 could be caused by two factors: i) a non-adequate segmentation model for the faults that considers too short fault sections and hence, higher earthquake rates than the catalogue, ii) the already acknowledged uncertainties and poor reliability of some geological fault data affecting the modelisation. Underestimation of the catalogue by hyp. 3 could be explained by the largest ruptures allowed in this model that may slightly contribute to limit the annual rates in the lower magnitudes. We are not able to distinguish the contribution of each option, but further research should focus first on exploring the impact of new segmentation models and second, on constraining critical fault parameters (i.e. slip rate) as is discussed in Sections 5.1.2 and 5.2.

Considering the consistency of the models with the catalogue, hyp. 2 should have more weight in a PSHA, followed by hyp. 1 and 3 similarly, and finally hyp. 4.

5.1.2. Paleorates

Recent studies on active faults at the EBSZ allowed to infer slip rates in specific portions of such faults as well as to calculate rates of earthquakes. In this study, the rates inferred from paleoseismology are a qualitative way to analyze the prediction of the models in the high magnitude range, where the seismic catalogue is not well represented. Similar to the case of the catalogue, the agreement or disagreement of the paleorates with the modelled rates does not provide a way to accept or rule out any of our hypotheses, but to weight them for future PSHA. Paleorates, though, have an additional problem related to the high uncertainties and low resolution of the paleoseismological data in the study area. One of these problems applies mainly to the magnitude of the events inferred from geological observations.

We considered that all the paleorates reflect earthquakes of $M_w \geq 6.25 \pm 0.25$. However, lower magnitude earthquakes can rupture the surface as well (i.e. the M_w 5.5 1975 Homestead Valley earthquake; Schwartz, 2018) implying that they could be observed in the EBSZ trenches and incorporated to the paleorate estimations as larger. This uncertainty has a difficult assessment at the EBSZ, although our magnitude threshold selection is supported by statistical observations of fault ruptures (see Section 3.2.2).

Another one affects directly the paleoearthquake rate estimations and concerns the fact that paleoseismology always provides a minimum number of paleoearthquakes and hence, maximum recurrence intervals. There are two main causes for this:

- The first is that paleoseismic studies are limited to specific regions and branches of a fault and rarely account for the whole structure. Surface ruptures are usually not continuous along strike and do not always accommodate ruptures on the same branch. Recent examples such as the 2016 M_w 7.8 Kaikoura earthquake (New Zealand) support this observation, where a significant part of the deformation was accommodated off-fault (e.g. Kearse et al., 2018). This way, the missing of events in the paleoseismic record is likely and higher paleorate values should be expected.
  Following this reasoning, our hyp. 4 is not suitable, since increased paleorates would lead to even much stronger disagreement with the modelled curves of such hypothesis. The strong underestimation of the paleorates by hyp. 4, together with its misfit with the catalogue and high %NMS suggesting modelling issues, lead us to estimate that this rupture hypothesis treats unrealistically long multi-fault rupture possibilities considering the data used and the rupture hypotheses explored.
- The second reason is linked to the lack of depositional continuity, as highlighted by Ortuño et al. (2012) in AMF-1. The discontinuous geological record hinders the identification and time constraining of the number of paleoseismic events observed and might lead to erroneous paleorate estimations. In Fig. 4, the paleorate from Ortuño et al. (2012) in AMF-1 is underestimated due to this effect, resulting in a misfit with the modelled MFDs of hyp. 1–3 and the paleorate by Martínez-Díaz et al. (2018).

Hyp. 2 and hyp. 3 both fit well with the paleorates suggesting that, given the inputs and rupture models explored, multi-fault rupture scenarios involving single or several whole faults allow to explain the paleoearthquake rate estimations. The paleorate fits of these hypotheses are consistent with their fits with the catalogue, especially hyp. 2 (Fig. 3). This enhances the robustness of these models.

Hyp. 1 performs good predictions of the paleorates as well, especially for AMF, but the fits are less consistent in general, compared to hyp. 2 and 3 (Fig. 4). It is important to recall that the most suitable hypothesis should agree not only with the rates of the higher magnitudes, but also with the rates of smaller magnitudes represented by the seismic catalogue. Hyp. 2 and hyp. 3 satisfy this requirement more correctly than hyp. 1 (Fig. 3) and accordingly should have more weight in subsequent PSHA. Similarly to the analysis with the catalogue, the weaker agreement of hyp. 1 with the paleorates could mean that either or both the segmentation proposed for these faults is not adequate and

larger ruptures should be expected (e.g. hyp. 2 and 3), and that paleoearthquake data is underestimated. Both epistemic uncertainties should be explored in further research, although the latter is more difficult to assess, since the issues are somehow inherent to the paleoseismic approaches. More paleoseismic research might help improve and better constrain paleoearthquake data at the EBSZ.

Finally, the method used to infer the paleorates in each study (Table 2) is conditioning the robustness of the results, because it affects the independence of the analysis. Martínez-Díaz et al. (2018) results are based in a single observed paleoevent in a trench. The paleorates are inferred using the geological moment rate from the fault slip rate and the seismic moment of the maximum expected rupture following the maximum magnitude model from Wesnousky (1986). Since SHERIFS uses slip rates as inputs, the models for this fault are somehow linked to the paleorates and the analysis cannot be claimed as completely independent. Martín-Banda et al. (2015) infer the paleorate for CAF-1 similarly, but the value is consistent with the one inferred independently from age constraints of paleoevents in trenches. Insua-Arévalo et al. (2015) for LTF, infer the slip rate of the fault from the paleorates and the offsets in the trenches. This dependence between models and data to weight them does not invalidate the analysis, though; the modelled MFDs are not build relying only on the exploration of slip rates but also on fault rupture scenarios (Mmax) and the b value, which in this case are independent variables.

In the other faults explored, the paleorate estimations (Table 2) are inferred from dividing the number of paleoevents in trenches over their observational time period, thus they are not dependent on the slip rate or maximum expected rupture; they are independent data to compare with the modelled earthquake rates.

5.2. Additional considerations on the modelling

The present study raised several critical questions concerning the databases that may be of interest for other low-strain regions similar to the EBSZ and for PSHA modelers.

SHERIFS constitutes a useful tool to discuss the epistemic uncertainties affecting a given fault system for fault source modelling in PSHA. In the particular case of the EBSZ, as in most low-strain regions, the main epistemic uncertainties are related to the geological fault input data used, especially affecting slip rate and paleoearthquake rate estimations, and the definition of fault rupture scenarios to be explored. In this sense, the results of this study, far from precisely determining the EBSZ behavior, have shown to be a practical tool to highlight where these uncertainties are more important and limiting. One clear example is PF, one of the less studied faults of the system with contrasting low slip rates (Table 1) that affect the modelling and the resulting distribution of hyp. 4. This highlights where future research should focus to better constrain these parameters and which rupture models are not adequate in the calculation given the input data. Despite this, geodetic data suggests that in the transect between PF and AMF (Fig. 1B), most part of the slip rate is absorbed by the latter (Echeverria et al., 2013), which could explain the low values assigned to PF. Knowing and assessing these uncertainties is critical to account for them in fault-based PSHA.

In addition and despite the limitations, SHERIFS is also a good tool to determine the weights that different fault source models should have in PSHA according to their consistency with the seismic catalogues and paleoseismic studies.

5.3. Perspectives

It is critical that researchers challenge classical segmentation models and consider faults as systems of geological structures that can interact. This is especially relevant in regions of distributed deformation along complex fault systems (e.g. Berryman et al., 2012) as it could be the case of the EBSZ, where the rupture models selected may have important repercussions on PSHA.

The research in this paper constitutes the first step for a fault-based PSHA at the EBSZ in which epistemic uncertainties of the available databases are discussed. Hence, further work needs to be focused towards reducing the uncertainties raised, especially from the geological and paleoseismic records. Moreover, the approach might serve as an example for similar seismo-tectonic contexts, as well as for defining deterministic earthquake-scenarios for engineering applications.

In further modellings and especially for PSHA we also find necessary to consider a portion of the seismicity from the catalogue as background in SHERIFS calculations. Clearly, not all the seismicity within the buffer area defined is generated by the faults in our models, especially smaller magnitudes (Fig. 1B). This is critical because it might directly affect the seismic hazard of the region for short or mid-term return periods.

In the models we explored a particular GR distribution; the one used for the Spanish seismic hazard map (IGN-UPM working group, 2013). Considering the data available from the catalogue and paleoseismic studies, we do not have clear criteria to dismiss it. However, other studies in other regions, for instance New Zealand (Stirling and Gerstenberger, 2018), have proved that GR distributions do not always describe annual rates of the high magnitudes derived from paleoseismic data. Exploring these options at the EBSZ in further research is also important due to its repercussions on the seismic hazard assessments.

6. Conclusions

In this study, we have modelled the magnitude-frequency distributions of the Eastern Betics Shear Zone (SE, Spain) using selected available geological data on faults and exploring four rupture hypotheses. The first hypothesis only allows ruptures within the extent of the segmentation proposed in literature and the other three allow multi-fault ruptures with maximum lengths that range from whole faults to nearly the whole system. Each hypothesis is defined based on selected geological rules.

The results suggest that the occurrence of multi-fault ruptures extending longer than the classic sections defined in the literature and involving individual whole faults or several whole faults (hypotheses 2 and 3, respectively) are consistent with both the seismic catalogue and the available paleoearthquake record. The other hypotheses, especially hypothesis 4, are less consistent with these data. Despite their different performance, no hypothesis can be completely ruled out because the resulting rates are dependent on the reliability and multiple epistemic uncertainties affecting the geological input data as well as the criteria on the definition of the hypotheses. Instead, they are weighted for further PSHA studies being hypothesis 2 and 3 the ones with higher weight.

The comprehensive methodology followed in this work, and particularly the use of SHERIFS, is revealed as a practical method for obtaining fault-system MFDs and as a practical tool for highlighting limitations and epistemic uncertainties in geological and paleoseismic data of the fault system to be assessed in further research. The main geological uncertainties are related to poorly constrained and unreliable slip rate estimations for some faults mainly due to lack of paleoseismic research. These data have a high impact on the modelling, since they limit the annual rates of earthquakes for some hypotheses. On the other hand, uncertainties from paleoseismic data might lead to wrong estimates of the rates of paleoearthquakes. Accounting and reducing these uncertainties are key issues for the improvement of fault-based PSHA.

Considering faults as interacting systems is an option that needs to be acknowledged when modelling seismic hazard, as evidenced by the recent experience from earthquakes worldwide. This means overcoming the classical sectioning models and exploring different multi-fault rupture models by combining seismic and paleoseismic data.

Declaration of competing interest

None.

Acknowledgements

This work was supported by the PREVENT project (CGL2015-66263-R) and FPI grant of Octavi Gómez-Novell (BES-2016-077048), funded by the Spanish Ministry of Science, Innovation and Universities. The authors want to thank the anonymous reviewers and the editor for the comments and suggestions that contributed to the improvement of the present manuscript, as well as the ESC Fault2SHA working group members for the fruitful discussions and work sessions that enhanced the quality of this study.

Appendix A. Information used to infer slip rate and paleorate data on each individual fault

This appendix contains details on what type of information the slip rate data and paleoearthquake rates (recurrences) are based on in each published study and for each fault. This follows the information highlighted in Tables 1 and 2 and the fault sections in Fig. 2A of the paper. We also put emphasis on the expert criteria followed to assign slip rate values to those faults where there is no published slip rate data available.

A) Faults whose slip rate data are directly extracted from published studies.

- *CF:* The lateral slip rate is inferred from geomorphological analysis onshore (CF-2, 3) and offshore (CF-1, 2), 3D paleoseismological studies (CF-3; Moreno, 2011; Moreno et al., 2015) and geodetic studies (CF-3; Echeverria et al., 2015). All three methods are coincident in the predicted slip rate values (1.2 ± 0.1 mm·yr^{-1}) and valid since the Pliocene but also for the Holocene. Net and lateral slip rate show similar values because 1) the vertical slip rate for this fault is one to two orders of magnitude lower than the lateral (0.01–0.3 mm·yr^{-1}; Moreno, 2011) and 2) the differences in the slip rate values are within the uncertainty range. Paleorates are estimated from trenching results (Masana et al., 2018; Moreno, 2011) in the northern branch of the two parallel strands that compose CF-3. In these studies, 7 or more paleoearthquakes since 191 kyr were identified. However, we considered the 3 last earthquakes for the last 41.5 kyr (Moreno, 2011), since the earthquake rates are increased for this time period.
- *PF-1 and 2:* The net slip rates used are the lower and upper values of the long-term uplift rates of lower-middle Pleistocene terraces and alluvial fan surfaces (see discussion in García-Mayordomo, 2005). This last study considers this fault as mainly dip-slip, but new recent data on PF (Roquero et al., 2019) suggest strike slip kinematics, which could change the net slip rate values significantly. There are no published paleoseismic studies available in this fault and hence no paleorate estimations to date.
- *LTF:* The net slip rate of this fault is inferred from recurrence estimations of at least 2 paleoearthquakes observed in paleoseismic trenches and respective offsets (Insua-Arévalo et al., 2015). The slip rate and paleorate estimations refer to the last 12 kyr.
- *CAF-1:* For this fault, the net slip rate is calculated from restoration of deformation of the top a distinctive sedimentary unit exposed in trenches and cropping out in the mountain slope (Red Unit; Martín-Banda et al., 2015). This is a long-term slip rate for the last 209.1 ± 6.2 kyr, which is the age of the Red Unit, but the slip rate value is consistent with the one obtained from offsets in younger units in the trenches for the last 6.9 ± 1.8 kyr (Martín-Banda et al., 2015). The paleorates from this study are calculated from the slip rate and seismic moment considering the rupture of the whole section. However, these paleorates are consistent with the ones estimated from two paleoevents for the last 6.0 kyr.
- *BSF-1 to 3:* The net slip rates of these fault sections are inferred from the uplift of 2–3 kyr old continental sedimentary units (Alfaro et al., 2012a). No paleoseismic trench studies are available for these faults.
- *AMF-1:* The lateral slip rate in this section is inferred from offsets in fluvial channels summed for all the branches that the fault shows (Ferrater, 2016; Ferrater et al., 2017). Vertical slip rate estimations in this section are subject to a larger uncertainty and the values are about one order of magnitude lower (0.16–0.22 mm·yr^{-1}; Ortuño et al., 2012), hence strike-slip is the predominant kinematics of the fault. The slip rate data are for the last 200 kyr. Recent paleoseismological studies in this section have also been able to identify paleoearthquakes in the southwestern tip (Ortuño et al., 2012) and historical earthquakes in the northeastern tip (Martínez-Díaz et al., 2018). The minimum paleorates inferred from paleoseismic studies in this section are for the last 116 kyr (Ortuño et al., 2012).
- *AMF-2:* The lateral slip rate (1.0 ± 0.2 mm·yr^{-1}) is inferred from offsets in fluvial channels for the last 30 kyr (Ferrater, 2016; Ferrater et al., 2017). Paleoseismological 3D trenching in this section inferred net slip rate values in the same range (0.9 ± 0.1 mm·yr^{-1} for the last 20 kyr; Ferrater, 2016), hence verical slip rate is negligible (0.1 ± 0.0 mm·yr^{-1}). Paleoseismological studies in this section identified a minimum of 10 paleoearthquakes for the last 59 kyr, which allowed to infer the respective paleorates.
- *AMF-4:* The net slip rate in this section is estimated from long term (since late Miocene-Pliocene) uplift through geological structural analysis in the mountain ranges limited by this section. These methods imply large uncertainties for the slip rate estimation, because factors such as sediment compaction need to be considered. Although the latest studies in this section infer better constrained values (0.13–0.18 mm·yr^{-1}; Herrero-Barbero et al., 2017) we used the wider range estimated in Herrero-Barbero (2016) (0.07–0.37 mm·yr^{-1}) to ensure a conservative margin of uncertainty.

B) Faults whose slip rate data are inferred following expert criteria or unpublished work.

- *PF-3:* Slip rate estimations for this fault section are not available, since there is no studies in this area. According to the values assigned, the slip rate increases from PF-1 and 2 to LTF. Thus, it is feasible that, in order to accommodate this difference, PF-3 has an intermediate slip rate. For this reason, we assigned to PF-3 a slip rate which is the mean between the values of PF-2 and LTF. The uncertainty range assigned is an intermediate value between the uncertainties of these two faults (Table 1).
- *CAF-2:* For this fault section there is a published net slip rate value of 0.54 mm·yr^{-1} (García-Mayordomo, 2005 and references), based on geomorphological offsets and tectonic uplift (at minimum since the last 160 kyr). However, ongoing research on this fault (Martín-Banda, personal communication) yields new slip rate values: 0.48–0.54 mm·yr^{-1}.
- *BSF-4:* This section of BSF is offshore and only a few studies have focused on that part of the fault, hence not enough data is available to do estimations of the slip rate of this section. Although some authors (e.g. Alfaro et al., 2012a) suggest that the deformation associated to the BSF decreases towards the E, from a conservative perspective we assigned the same slip rate range as for BSF-3 (0.12–0.3 mm·yr^{-1}), which is consistent with new GPS results in that sector (Borque et al., 2019).
- *AMF-3:* There are no slip rate estimations for this section. In fact, the geomorphological expression of this fault is scarce and hence its slip rate is probably much lower than the other sections. Since it is our only source of information, we used the net slip rate estimated in the QAFI database (0.042–0.097 mm·yr^{-1}) for AMF-3, rounded the

upper uncertainty value and enlarged considerably the lower bound uncertainty, obtaining a net slip rate range of 0.01–0.1 mm·yr^{-1}. From our perspective, enlarging the uncertainties accounts for a more conservative way to express the lack of knowledge of this fault.

References

Alfaro, P., Bartolomé, R., Borque, M.J., Estévez, A., García-Mayordomo, J., García-Tortosa, F.J., Gil, A.J., Gràcia, E., Lo Iacono, C., Perea, H., 2012a. The Bajo Segura Fault Zone: active blind thrusting in the Eastern Betic Cordillera (SE Spain). J. Iber. Geol. 38. https://doi.org/10.5209/rev_JIGE.2012.v38.n1.39217.

Alfaro, P., Delgado, J., García-Tortosa, F.J., Lenti, L., López, J.A., López-Casado, C., Martino, S., 2012b. Widespread landslides induced by the Mw 5.1 earthquake of 11 May 2011 in Lorca, SE Spain. Eng. Geol. 137–138, 40–52. https://doi.org/10.1016/j.enggeo.2012.04.002.

Argus, D.F., Gordon, R.G., DeMets, C., 2011. Geologically current motion of 56 plates relative to the no – net – rotation reference frame. Geochem. Geophys. Geosyst. 12, 1–13. https://doi.org/10.1029/2011GC003751.

Baize, S., Nurminen, F., Sarmiento, A., Dawson, T., Takao, M., Scotti, O., Azuma, T., Boncio, P., Champenois, J., Cinti, F.R., Civico, R., Costa, C., Guerrieri, L., Marti, E., McCalpin, J., Okumura, K., Villamor, P., 2019. A worldwide and unified database of surface ruptures (SURE) for fault displacement hazard analyses. Seismol. Res. Lett. https://doi.org/10.1785/0220190144.

Baumont, D., Scotti, O., Courboulex, F., Melis, N., 2004. Complex kinematic rupture of the Mw 5.9, 1999 Athens earthquake as revealed by the joint inversion of regional seismological and SAR data. Geophys. J. Int. 158, 1078–1087. https://doi.org/10.1111/j.1365-246X.2004.02374.x.

Bayrak, Y., Öztürk, S., Çinar, H., Kalafat, D., Tsapanos, T.M., Koravos, G.C., Leventakis, G.A., 2009. Estimating earthquake hazard parameters from instrumental data for different regions in and around Turkey. Eng. Geol. 105, 200–210. https://doi.org/10.1016/j.enggeo.2009.02.004.

Berryman, K.R., Cochran, U.A., Clark, K.J., Biasi, G.P., Langridge, R.M., Villamor, P., 2012. Major earthquakes occur regularly on an isolated plate boundary fault. Science 336, 1690 LP–1693. https://doi.org/10.1126/science.1218959.

Biasi, G.P., Weldon, R.J., 2006. Estimating surface rupture length and magnitude of paleoearthquakes from point measurements of rupture displacement. Bull. Seismol. Soc. Am. 96, 1612–1623. https://doi.org/10.1785/0120040172.

Boncio, P., Lavecchia, G., Pace, B., 2004. Defining a model of 3D seismogenic sources for Seismic Hazard Assessment applications: the case of central Apennines (Italy). J. Seismol. 8, 407–425. https://doi.org/10.1023/B:JOSE.0000038449.78801.05.

Bonilla, M.G., 1982. Evaluation of Potential Surface Faulting and Other Tectonic Deformation. USGS Open-File Report 82-732.

Borque, M.J., Sánchez-Alzola, A., Martin-Rojas, I., Alfaro, P., Molina, S., Rosa-Cintas, S., Rodríguez-Caderot, G., de Lacy, C., Avilés, M., Herrera-Olmo, A., García-Tortosa, F.J., Estévez, A., Gil, A.J., 2019. How much Nubia-Eurasia convergence is accommodated by the NE end of the Eastern Betic Shear Zone (SE Spain)? Constraints from GPS velocities. Tectonics 38, 1824–1839. https://doi.org/10.1029/2018TC004970.

Bousquet, J.C., 1979. Quaternary strike-slip faults in Southeastern Spain. Dev. Geotecton. 13, 277–286. https://doi.org/10.1016/B978-0-444-41783-1.50044-1.

Chartier, T., Scotti, O., Lyon-Caen, H., Boiselet, A., 2017. Methodology for earthquake rupture rate estimates of fault networks: example for the western Corinth rift, Greece. Nat. Hazards Earth Syst. Sci. 17, 1857–1869. https://doi.org/10.5194/nhess-17-1857-2017.

Chartier, T., Scotti, O., Lyon-Caen, H., 2019. SHERIFS: open-source code for computing earthquake rates in fault systems and constructing hazard models. Seismol. Res. Lett. https://doi.org/10.1785/0220180332.

Cornell, C.A., 1968. Engineering seismic risk analysis. Bull. Seismol. Soc. Am. 58, 1583–1606.

De Larouzière, F.D., Bolze, J., Bordet, P., Hernandez, J., Montenat, C., Ott d'Estevou, P., 1988. The Betic segment of the lithospheric Trans-Alboran shear zone during the Late Miocene. Tectonophysics 152, 41–52. https://doi.org/10.1016/0040-1951(88)90028-5.

Delgado, J., Peláez, J.A., Tomás, R., García-Tortosa, F.J., Alfaro, P., López Casado, C., 2011. Seismically-induced landslides in the Betic Cordillera (S Spain). Soil Dyn. Earthq. Eng. 31, 1203–1211. https://doi.org/10.1016/j.soildyn.2011.04.008.

Demets, C., Gordon, R.G., Argus, D.F., 2010. Geologically current plate motions. Geophys. J. Int. 181, 1–80. https://doi.org/10.1111/j.1365-246X.2009.04491.x.

Echeverria, A., Khazaradze, G., Asensio, E., Gárate, J., Dávila, J.M., Suriñach, E., 2013. Crustal deformation in eastern Betics from CuaTeNeo GPS network. Tectonophysics 608, 600–612. https://doi.org/10.1016/j.tecto.2013.08.020.

Echeverria, A., Khazaradze, G., Asensio, E., Masana, E., 2015. Geodetic evidence for continuing tectonic activity of the Carboneras fault (SE Spain). Tectonophysics 663, 302–309. https://doi.org/10.1016/J.TECTO.2015.08.009.

Ferrater, M., 2016. Velocitat de desplaçament de la falla d'Alhama de Murcia (Bètiques Orientals); implicacions en el seu potencial sísmic. PhD thesis. Universitat de Barcelona, Barcelona, Spain.

Ferrater, M., Ortuño, M., Masana, E., Martínez-Díaz, J.J., Pallàs, R., Perea, H., Baize, S., García-Meléndez, E., Echeverria, A., Rockwell, T., Sharp, W.D., Arrowsmith, R., 2017. Lateral slip rate of Alhama de Murcia fault (SE Iberian Peninsula) based on a morphotectonic analysis: comparison with paleoseismological data. Quat. Int. 451, 87–100. https://doi.org/10.1016/j.quaint.2017.02.018.

Field, E., Biasi, G.P., Bird, P., Dawson, T.E., Felzer, K.R., Jackson, D.D., Johnson, K.M., Jordan, T.H., Madden, C., Michael, A.J., Milner, K., Page, M.T., Parsons, T., Powers, P.M., Shaw, B.E., Thatcher, W.R., Weldon, R.J., Zeng, Y., 2014. The uniform California earthquake rupture forecast, version 3 (UCERF3). Bull. Seismol. Soc. Am. 3, 1122–1180. https://doi.org/10.3133/ofr20131165.

Frankel, A., 1995. Mapping seismic hazard in the central and eastern United States. Seismol. Res. Lett. 66, 8–21. https://doi.org/10.1785/gssrl.66.4.8.

García-Mayordomo, J., 2005. Caracterización y analisis de la peligrosidad sismica en el sureste de España. PhD thesis. Universidad Complutense de Madrid, Madrid, Spain.

García-Mayordomo, J., 2015. Creación de un modelo de zonas sismogénicas para el cálculo del mapa de peligrosidad sísmica de España. Madrid.

García-Mayordomo, J., Gaspar-Escribano, J.M., Benito, B., 2007. Seismic hazard assessment of the Province of Murcia (SE Spain): analysis of source contribution to hazard. J. Seismol. 11, 453–471. https://doi.org/10.1007/s10950-007-9064-0.

García-Mayordomo, J., Insúa-Arévalo, J.M., Martínez-Díaz, J.J., Jiménez-Díaz, A., Alvárez-Gomez, J.A., Pérez-López, R., Rodríguez-Pascua, M.A., Martín-González, F., Giner-Robles, J., Masana, E., Nemser, E., Cabral, J., 2012. The quaternary active faults database of Iberia v 0.1. J. Iber. Geol. 38, 285–302. https://doi.org/10.5209/rev_JIGE.2012.v38.n1.39219.

García-Mayordomo, J., Martín-Banda, R., Insua-Arévalo, J.M., Álvarez-Gómez, J.A., Martínez-DIáz, J.J., Cabral, J., 2017. Active fault databases: building a bridge between earthquake geologists and seismic hazard practitioners, the case of the QAFI v.3 database. Nat. Hazards Earth Syst. Sci. 17, 1447–1459. https://doi.org/10.5194/nhess-17-1447-2017.

García-Mayordomo, J., Ortuño, M., Insua-Arévalo, J.M., Scotti, O., Visini, F., Fault2SHA-Betics Working Group, 2018. The Fault2SHA-Betics Working Group: Promoting knowledge interchange between earthquake geologists and seismic hazard modellers in the Eastern Betics (SE Spain). In: Resúmenes de La 3ª Reunión Ibérica Sobre Fallas Activas y Paleosismología, Alicante, España, pp. 243–246.

Gaspar-Escribano, J.M., Benito, B., García-Mayordomo, J., 2008. Hazard-consistent response spectra in the Region of Murcia (Southeast Spain): comparison to earthquake-resistant provisions. Bull. Earthq. Eng. 6, 179–196.

Gaspar-Escribano, J.M., Rivas-Medina, A., Parra, H., Cabañas, L., Benito, B., Ruiz Barajas, S., Martínez Solares, J.M., 2015. Uncertainty assessment for the seismic hazard map of Spain. Eng. Geol. 199, 62–73. https://doi.org/10.1016/j.enggeo.2015.10.001.

Gómez-Novell, O., Chartier, T., García-Mayordomo, J., Ortuño, M., Masana, E., Insua-Arévalo, J.M., Scotti, O., 2019. Modelling earthquake multi-fault ruptures across complex fault systems for probabilistic seismic hazard assessment: the Eastern Betics Shear Zone. [WWW Document]. Mendeley Data v1. https://doi.org/10.17632/pt32rrncdm.1.

Gutenberg, B., Richter, C.F., 1944. Frequency of earthquakes in California. Bull. Seismol. Soc. Am. 34, 185–188.

Herrero-Barbero, P., 2016. Análisis estructural del segmento Alhama – Alcantarilla de la Falla de Alhama de Murcia y sus implicaciones en el Riesgo Análisis estructural del segmento Alhama – Alcantarilla de la Falla de Alhama de Murcia y sus implicaciones en el Riesgo Sísmico. Universidad Complutense de Madrid.

Herrero-Barbero, P., Álvarez-Gómez, J.A., Martínez-Díaz, J.J., 2017. Análisis estructural en el segmento Alhama de Murcia – Alcantarilla (Falla de Alhama de Murcia) y sus implicaciones en la peligrosidad sísmica. Geogaceta 62, 11–14.

IGME, 2015a. QAFI v.3: Quaternary Active Faults Database of Iberia. [WWW Document]. URL. http://info.igme.es/qafi accessed 6.27.19.

IGME, 2015b. ZESIS: Base de Datos de Zonas Sismogénicas de la Península Ibérica y territorios de influencia para el cálculo de la peligrosidad sísmica en España. [WWW Document]. URL. http://info.igme.es/zesis accessed 6.27.19.

IGN-UPM working group, 2013. Actualización de mapas de peligrosidad sísmica de España 2012. Centro Nacional de Información Geográfica. Instituto Geográfico Nacional, Madrid.

Insua-Arévalo, J.M., García-Mayordomo, J., Salazar, A.E., Rodríguez-Escudero, E., Martín-Banda, R., Álvarez-Gómez, J.A., Canora, C., Martínez-Díaz, J.J., 2015. Paleoseismological evidence of holocene activity of the los tollos fault (Murcia, SE Spain): a lately formed quaternary tectonic feature of the eastern betic shear zone. J. Iber. Geol. 41, 333–350. https://doi.org/10.5209/rev_JIGE.2015.v41.n3.49948.

Kearse, J., Little, T.A., Van Dissen, R.J., Barnes, P.M., Langridge, R., Mountjoy, J., Ries, W., Villamor, P., Clark, K.J., Benson, A., Lamarche, G., Hill, M., Hemphill-Haley, M., 2018. Onshore to offshore ground-surface and seabed rupture of the Jordan–Kekerengu–Needles fault network during the 2016 Mw 7.8 Kaikoura earthquake, New Zealand. Bull. Seismol. Soc. Am. 108, 1573–1595. https://doi.org/10.1785/0120170304.

Langridge, R.M., Rowland, J., Villamor, P., Mountjoy, J., Townsend, D.B., Nissen, E., Madugo, C., Ries, W.F., Gasston, C., Canva, A., Hatem, A.E., Hamling, I., 2018. Coseismic rupture and preliminary slip estimates for the Papatea fault and its role in the 2016 mw 7.8 Kaikōura, New Zealand, earthquake. Bull. Seismol. Soc. Am. 108, 1596–1622. https://doi.org/10.1785/0120170336.

Leonard, M., 2010. Earthquake fault scaling: self-consistent relating of rupture length, width, average displacement, and moment release. Bull. Seismol. Soc. Am. 100, 1971–1988. https://doi.org/10.1785/0120090189.

Little, T.A., van Dissen, R., Kearse, J., Norton, K., Benson, A., Wang, N., 2018. Kekerengu fault, New Zealand: timing and size of late holocene surface ruptures. Bull. Seismol. Soc. Am. 108, 1556–1572. https://doi.org/10.1785/0120170152.

Magrin, A., Peresan, A., Kronrod, T., Vaccari, F., Panza, G.F., 2017. Neo-deterministic seismic hazard assessment and earthquake occurrence rate. Eng. Geol. 229, 95–109. https://doi.org/10.1016/j.enggeo.2017.09.004.

Malservisi, R., Furlong, K.P., Gans, C.R., 2005. Microseismicity and creeping faults: Hints from modeling the Hayward fault, California (USA). Earth Planet. Sci. Lett. 235, 421–435. https://doi.org/10.1029/2000jb000084.

Martín-Banda, R., García-Mayordomo, J., Insua-Arévalo, J.M., Salazar, A.E., Rodríguez-Escudero, E., Álvarez-Gómez, J.A., Medialdea, A., Herrero, M.J., 2015. New insights on the seismogenic potential of the Eastern Betic Shear Zone (SE Iberia): quaternary activity and paleoseismicity of the SW segment of the Carrascoy Fault Zone. Tectonics

35, 55–75. https://doi.org/10.1002/2015TC003997.
Martínez-Díaz, J.J., 1998. Neotectónica y Tectónica Activa del Sector Centro-Occidental de la Región de Murcia y Sur de Almería (Cordillera Bética – España). PhD thesis. Universidad Complutense de Madrid, Madrid, Spain.
Martínez-Díaz, J.J., Masana, E., Hernández-Enrile, J.L., Santanach, P., 2003. Effects of repeated paleoearthquakes on the Alhama de Murcia Fault (Betic Cordillera, Spain) on the quaternary evolution of an alluvial fan system. Ann. Geophys. 46, 775–791. https://doi.org/10.4401/ag-3455.
Martínez-Díaz, J.J., Bejar-Pizarro, M., Álvarez-Gómez, J.A., Mancilla, F.L., Stich, D., Herrera, G., Morales, J., 2012EEa. Tectonic and seismic implications of an intersegment rupture. the damaging May 11th 2011 Mw 5.2 Lorca, Spain, earthquake. Tectonophysics 546–547, 28–37. https://doi.org/10.1016/j.tecto.2012.04.010.
Martínez-Díaz, J.J., Masana, E., Ortuño, M., 2012EEb. Active tectonics of the Alhama de Murcia fault, Betic Cordillera, Spain. J. Iber. Geol. 38, 253–270. https://doi.org/10.5209/rev_JIGE.2012.v38.n1.39218.
Martínez-Díaz, J.J., Alonso-Henar, J., Insua-Arévalo, J.M., Canora, C., García-Mayordomo, J., Rodríguez-Escudero, E., Álvarez-Gómez, J.A., Ferrater, M., Ortuño, M., Masana, E., 2018. Geological evidences of surface rupture related to a seventeenth century destructive earthquake in Betic Cordillera (SE Spain): constraining the seismic hazard of the Alhama de Murcia fault. J. Iber. Geol. https://doi.org/10.1007/s41513-018-0082-2.
Masana, E., Martínez-Díaz, J.J., Hernández-Enrile, J.L., Santanach, P., 2004. The Alhama de Murcia fault (SE Spain), a seismogenic fault in a diffuse plate boundary: seismotectonic implications for the Ibero-Magrebian region. J. Geophys. Res. Solid Earth 109, 1–17. https://doi.org/10.1029/2002JB002359.
Masana, E., Moreno, X., Gràcia, E., Pallàs, R., Ortuño, M., López, R., Gómez-Novell, O., Ruano, P., Perea, H., Štěpančíková, P., Khazaradze, G., 2018. First evidence of paleoearthquakes along the Carboneras Fault Zone (SE Iberian Peninsula): Los Trances site. Geol. Acta 16, 461–476. https://doi.org/10.1344/GeologicaActa2018.16.4.8.
McCalpin, J., 1996. Paleoseismology. Academic Press.
McGuire, R.K., 1976. EQRISK Evaluation of Sites for Earthquake Risk. USGS Open-File Report 76-67.
Moreno, X., 2011. Neotectonic and Paleoseismic Onshore-Offshore Integrated Study of the Carboneras Fault (Eastern Betics, SE Iberia). PhD thesis. Universitat de Barcelona, Barcelona, Spain.
Moreno, X., Masana, E., Pallàs, R., Gràcia, E., Rodés, Á., Bordonau, J., 2015. Quaternary tectonic activity of the Carboneras Fault in the La Serrata range (SE Iberia): geomorphological and chronological constraints. Tectonophysics 663, 78–94. https://doi.org/10.1016/j.tecto.2015.08.016.
Ortuño, M., Masana, E., García-Meléndez, E., Martínez-Díaz, J.J., Štěpančíková, P., Cunha, P.P., Sohbati, R., Canora, C., Buylaert, J.P., Murray, A.S., 2012. An exceptionally long paleoseismic record of a slow-moving fault: the Alhama de Murcia fault (Eastern Betic shear zone, Spain). Bull. Geol. Soc. Am. 124, 1474–1494. https://doi.org/10.1130/B30558.1.
Pedrera, A., Galindo-Zaldívar, J., Marín-Lechado, C., García-Tortosa, F.J., Ruano, P., Garrido, A.C., Azañón, J.M., Peláez, J.A., Giaconia, F., 2012. Recent and active faults and folds in the central-eastern Internal Zones of the Betic Cordillera. J. Iber. Geol. 38, 191–208. https://doi.org/10.5209/rev_JIGE.2012.v38.n1.39213.
Peláez, J.A., Delgado, J., López Casado, C., 2005. A preliminary probabilistic seismic hazard assessment in terms of Arias intensity in southeastern Spain. Eng. Geol. 77, 139–151. https://doi.org/10.1016/j.enggeo.2004.09.002.
Rastgoo, M., Rahimi, H., Romanelli, F., Vaccari, F., Panza, G.F., 2018. Neo-deterministic seismic hazard assessment for Alborz Region, Iran. Eng. Geol. 242, 70–80. https://doi.org/10.1016/j.enggeo.2018.05.025.
Rivas-Medina, A., Benito, B., Miguel Gaspar-Escribano, J., 2018. Approach for combining fault and area sources in seismic hazard assessment: application in south-eastern Spain. Nat. Hazards Earth Syst. Sci. 18, 2809–2823. https://doi.org/10.5194/nhess-18-2809-2018.
Roquero, E., Silva, P.G., Rodríguez-Pascua, M.A., Bardají, T., Elez, J., Carrasco-García, P., Giner-Robles, J.L., 2019. Analysis of faulted fan surfaces and paleosols in the Palomares Fault Zone (Betic Cordillera, SE Spain): paleoclimatic and paleoseismic implications. Geomorphology 342, 88–102. https://doi.org/10.1016/j.geomorph.2019.06.003.
Scholz, C.H., 1990. The Mechanics of Earthquakes and Faulting. Cambridge University Press, Cambridge, United Kingdom. https://doi.org/10.1017/9781316681473.
Schwartz, D.P., 2018. Review: past and future fault rupture lengths in seismic source characterization-the long and short of it. Bull. Seismol. Soc. Am. 108, 2493–2520. https://doi.org/10.1785/0120160110.
Schwartz, D.P., Coppersmith, K.J., 1984. Fault behavior and characteristic earthquakes: examples from the Wasatch and San Andreas fault zones. J. Geophys. Res. Solid Earth 89, 5681–5698.
Shen, Z.K., Jackson, D.D., Feng, Y.J., Cline, M., Kim, M., Fang, P., Bock, Y., 1994. Postseismic deformation following the landers earthquake, California, 28 June 1992. Bull. Seismol. Soc. Am. 84, 780–791. https://doi.org/10.1029/97JB00210.
Silva, P.G., Goy, J.L., Somoza, L., Zazo, C., Bardají, T., 1993. Landscape response to strike-slip faulting linked to collisional settings: quaternary tectonics and basin formation in the Eastern Betics, southeastern Spain. Tectonophysics 224, 289–303. https://doi.org/10.1016/0040-1951(93)90034-H.
Stein, R.S., Lisowski, M., 1983. The 1979 homestead valley earthquake sequence, California: control of aftershocks and postseismic deformation. J. Geophys. Res. Solid Earth 88, 6477–6490.
Stich, D., Martín, J.B., Morales, J., 2007. Deformación sísmica y asísmica en la zona Béticas-Rif-Alborán. Rev. Soc. Geol. Esp. 20, 311–320.
Stich, D., Martín, R., Morales, J., 2010. Moment tensor inversion for Iberia-Maghreb earthquakes 2005–2008. Tectonophysics 483, 390–398. https://doi.org/10.1016/j.tecto.2009.11.006.
Stirling, M., Gerstenberger, M., 2018. Applicability of the Gutenberg–Richter relation for major active faults in New Zealand. Bull. Seismol. Soc. Am. 108, 718–728. https://doi.org/10.1785/0120160257.
Valentini, A., Visini, F., Pace, B., 2017. Integrating faults and past earthquakes into a probabilistic seismic hazard model for peninsular Italy. Nat. Hazards Earth Syst. Sci. 17, 2017–2039. https://doi.org/10.5194/nhess-17-2017-2017.
Wang, J.P., Lin, C.W., Taheri, H., Chan, W.S., 2012. Impact of fault parameter uncertainties on earthquake recurrence probability examined by Monte Carlo simulation – an example in Central Taiwan. Eng. Geol. 126, 67–74. https://doi.org/10.1016/j.enggeo.2011.12.012.
Wei, S., Fielding, E., Leprince, S., Sladen, A., Avouac, J.P., Helmberger, D., Hauksson, E., Chu, R., Simons, M., Hudnut, K., Herring, T., Briggs, R., 2011. Superficial simplicity of the 2010 El Mayorg-Cucapah earthquake of Baja California in Mexico. Nat. Geosci. 4, 615–618. https://doi.org/10.1038/ngeo1213.
Wells, D.L., Coppersmith, K.J., 1994. New empirical relationships among magnitude, rupture length, rupture width, rupture area, and surface displacements. Bull. Seismol. Soc. Am. 84, 974–1002.
Wesnousky, S.G., 1986. Earthquakes, quaternary faults, and seismic hazard in California. J. Geophys. Res. 91, 12587–12631. https://doi.org/10.1029/JB091iB12p12587.
Wesnousky, S.G., 2008. Displacement and geometrical characteristics of earthquake surface ruptures: issues and implications for seismic-hazard analysis and the process of earthquake rupture. Bull. Seismol. Soc. Am. 98, 1609–1632. https://doi.org/10.1785/0120070111.
Woessner, J., Laurentiu, D., Giardini, D., Crowley, H., Cotton, F., Grünthal, G., Valensise, G., Arvidsson, R., Basili, R., Demircioglu, M.B., Hiemer, S., Meletti, C., Musson, R.W., Rovida, A.N., Sesetyan, K., Stucchi, M., 2015. The 2013 European Seismic Hazard Model: key components and results. Bull. Earthq. Eng. 13, 3553–3596. https://doi.org/10.1007/s10518-015-9795-1.
Working Group On California Earthquake Probabilities, 2003. Earthquake Probabilities in the San Francisco Bay Region: 2002–2031. USGS Open-File Report 03-214.
Youngs, R.R., Coppersmith, K.J., 1985. Implications of fault slip rates and earthquake recurrence models to probabilistic seismic hazard estimates. Int. J. Rock Mech. Min. Sci. Geomech. Abstr. 23, 125. https://doi.org/10.1016/0148-9062(86)90651-0.